Solution-Based Group 14 Zintl Anions: New Frontiers and Discoveries

Yi Wang, John E. McGrady, and Zhong-Ming Sun*

Read Online

ACCESS | ill Metrics & More | Article Recommendations

CONSPECTUS: Group 14 Zintl anions $[E_x]^{q-}$ (E = Si–Pb, x = 4, 5, 9, 10) are synthetically accessible, and their diverse chemical reactivity makes them valuable synthons in the construction of larger nanoclusters with remarkable structures, intriguing patterns of chemical bonding, and tunable physical and chemical properties. A plethora of novel cluster anions have now been isolated from the reactions of polyanionic $[E_x]^{q-}$ precursors with low-valent d-/f-block metal complexes, main-group organometallics, or organics in polar aprotic solvents. The range of products includes intermetalloid clusters with transition metal atom(s) embedded in main-group element cages, organometallic Zintl anions in which $[E_x]^{q-}$ acts as a ligand, intermetallic Zintl anions where $[E_x]^{q-}$ is bridged by ligand-free transition metal atom(s), organo-Zintl anions where $[E_x]^{q-}$ is functionalized with organic-group(s), and oligomers formed through oxidative coupling reactions. The synthesis and characterization of these unconventional complexes, where important contributions to stability come from ionic, covalent, and metal–metal bonds as well as weaker aurophilic and van der Waals interactions, extend the boundaries of coordination chemistry and solid-state chemistry. Substantial progress has been made in this field over the past two decades, but there are still many mysteries to unravel related to the cluster growth mechanism and the controllable synthesis of targeted clusters, along with the remarkable and diverse patterns of chemical bonding that present a substantial challenge to theory. In this Account, we hope to shed some light on the relationship between structure, electronic properties, and cluster growth by highlighting selected examples from our recent work on homoatomic deltahedral $[E_x]^{q-}$ anions, including (1) germanium-based Zintl clusters, such as the supertetrahedral intermetallic clusters $[M_6Ge_{16}]^{4-}$ (M = Zn, Cd) and the sandwich cluster $\{(Ge_9)_2[\eta^6\text{-}Ge(PdPPh_3)_3]\}^{4-}$ with a heterometallic Ge@Pd$_3$ interlayer; (2) tin-based intermetalloid clusters $[M_x@Sn_y]^{q-}$ and the application of $[Co@Sn9]^{4-}$ in bottom-up synthesis; and (3) lead clusters with precious metal cores, including the largest Zintl anion $[Au_{12}Pb_{44}]^{8-}$. In addition to their intrinsic appeal from a structural and electronic perspective, these new cluster anions also show promise as precursors for the development of new materials with applications in heterogeneous catalysis, where we have recently reported the selective reduction of CO_2.
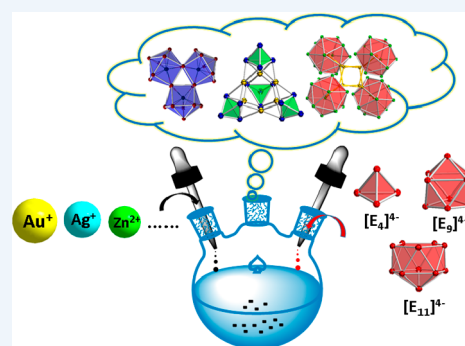
KEY REFERENCES

- Shu, C.; Morgan, H. W. T.; Qiao, L.; McGrady, J. E.; Sun, Z. A family of lead clusters with precious metal cores. *Nature Commun.* **2020**, *11*, 3477. The first *nido* icosahedral $[Ag@Pb_{11}]^{3-}$ and the largest Au–Pb intermetallic clusters, $[Au_8Pb_{33}]^{6-}$ and $[Au_{12}Pb_{44}]^{8-}$, were synthesized and fully characterized, and the secondary π-type Pb···Au interactions were shown to play an important role in stabilizing the clusters.[1]

- Xu, H.; Popov, I.; Tkachenko, N.; Wang, Z.; Muñoz-Castro, A.; Boldyrev, A.; Sun, Z. σ-aromaticity-induced stabilization of heterometallic supertetrahedral clusters $[Zn_6Ge_{16}]^{4-}$ and $[Cd_6Ge_{16}]^{4-}$. *Angew. Chem. Int. Ed.* **2020**, *59*, 17286–17290. Two heterometallic super-tetrahedral clusters were constructed from the tetrahedral cluster anion $[Ge_4]^{4-}$ and transition metal cations M^{2+} (M = Zn, Cd), with the stability arising from the formation of delocalized 3c-2e MGe$_2$ σ bonds.[2]

- Qiao, L.; Zhang, C.; Shu, C.; Morgan, H. W. T.; McGrady, J. E.; Sun, Z. $[Cu_4@E_{18}]^{4-}$ (E = Sn, Pb): Fused derivatives of endohedral stannaspherene and plumbaspherene. *J. Am. Chem. Soc.* **2020**, *142*, 13288–13293. Two intermetalloid Zintl clusters $[Cu_4@E_{18}]^{4-}$ (E = Sn, Pb), with a rhombic Cu$_4$ unit embedded inside continuous tetrel cages, were characterized.[3]

- Xu, H.; Tkachenko, N.; Wang, Z.; Chen, W.; Qiao, L.; Muñoz-Castro, A.; Boldyrev, A.; Sun, Z. A sandwich-type cluster containing $Ge@Pd_3$ planar fragment flanked by aromatic nonagermanide caps. *Nat. Commun.* **2020**, *11*, 5286. A heteroatomic metal cluster fragment $Ge@Pd_3$, with a central germanium atom in the zero oxidation state, was sandwiched between two $[Ge_9]^{2-}$ clusters.[4]

1. INTRODUCTION

The family of Zintl anions, naked polyanions of main-group elements, was named after the German chemist Eduard Zintl who first identified their presence in a liquid ammonia solution containing both post-transition metals or semimetals and alkali metals.[5] His name is also associated with the Zintl phases, salt-like polar intermetallics formed from the reaction of an electropositive s-block element with a more electronegative p-block metal or semimetal. Despite the shared name, these two classes of compounds were thought to be quite distinct until the discovery of the Zintl phase "Cs_4Ge_9" which contains a $[Ge_9]^{4-}$ anion that is well-known in the solution phase,[6] an observation that suggested a general synthetic route to solution-phase Zintl anions via extraction from soild-state Zintl phases. The ready accessibility of Zintl anions via this route has subsequently led to an extensive solution-phase Zintl anion chemistry, with the first example being the $[(\eta^4-Sn_9)Cr(CO)_3]^{4-}$ cluster where the labile mesityl ligand of $Cr(CO)_3(mes)$ (mes = η^6-l,3,5-$C_6Me_3H_3$) is displaced by the Zintl anion $[Sn_9]^{4-}$.[7] Many derivatives of the $[E_x]^{q-}$ anions have since been developed, each one with a fascinating structure and each posing an intriguing challenge to established theories of chemical bonding. These compounds can broadly be divided into four distinct categories:

(1) intermetalloid clusters containing at least two different (semi-) metals, often with one or more endohedral metal atom(s) within a deltahedral or 3-connected single cage[8-17]

(2) functionalized clusters with main-group organometallics, organics, or transition metal fragments with/without insertion of metal atom(s)[18-23]

(3) larger clusters generated by oxidative coupling reactions[24,25]

(4) ligand-free transition metal complexes where Zintl anions $[E_x]^{q-}$ are bridged by metal cation(s)[26-28]

A number of recent reviews have summarized important advances in this field and also posed important challenges to both synthetic and theoretical chemists.[29-32] Among these challenges, perhaps the most pressing is a lack of knowledge on the precise mechanisms by which these clusters are formed: in the absence of this knowledge, controllable synthesis remains a frustratingly elusive goal. We anticipate that ongoing research into the reactivities of $[E_x]^{q-}$ anions (E = Si–Pb, x = 4, 5, 9, 10) will go some way toward filling this void. At the present time, no more than three transition metal atoms have been embedded in a single tetrel cage, and the maximum size of tin- and lead-based Zintl clusters appears to be around 20, as exemplified by $[Ni_3@Ge_{18}]^{4-}$,[10] $[Pd_2@Sn_{18}]^{4-}$,[12] and $[Pb_9-Cd-Cd-Pb_9]^{6-}$, respectively.[33] The interplay between theory and experiment also continues to provide new directions for synthetic inquiry. For example, the icosahedral $[M@E_{12}]^{q-}$ cluster is almost ubiquitous in Sn and Pb chemistry, but no germanium analogues are known despite the fact that they have been shown to be stable.[34] Motivated by these and other questions, our lab continues to explore fundamental studies in this very active field,

and a series of unprecedented discoveries will be outlined in this Account.

2. GERMANIUM CLUSTER CHEMISTRY: NEW DISCOVERIES

Tetrahedral $[E_4]^{4-}$ ions have long been known in the solid-state where they are formed in reactions between alkali metals and the tetrels,[35] but they were first isolated from solution only in 2009 when Korber and co-workers obtained crystals of $A_4[E_4]$ (E = Sn, Pb; A = Rb, Cs) from liquid ammonia solution.[36] The dearth of tetrahedral $[E_4]^{4-}$-based species[37,38] stands in stark contrast to the extensive coordination chemistry of isoelectronic and isostructural P_4 and also to the rich chemistry of $[E_9]^{4-}$ alluded to previously.

The obstacles to developing the chemistry of the $[E_4]^{4-}$ unit may simply reflect their high charge:size ratio and consequent low solubility in commonly used library solvents such as tetrahydrofuran (THF), *N,N*-dimethylformamide (DMF), acetonitrile (CH_3CN), pyridine, and ethylenediamine (en). Recently, however, we have isolated the tetrahedral $[Ge_4]^{4-}$ unit in the intermetallic supertetrahedral clusters, $[Zn_6Ge_{16}]^{4-}$ and $[Cd_6Ge_{16}]^{4-}$. These compounds emerged during the course of our exploration of the reactivity of the solid-state precursor "$K_{12}Ge_{17}$" which contains one $[Ge_9]^{4-}$ and two $[Ge_4]^{4-}$ anions.[2] The cluster anions $[M_6Ge_{16}]^{4-}$ (M = Zn, Cd) are formed in the reaction of this precursor with $ZnMes_2$ or $CdMes_2$ (Mes = 2, 4, 6-$Me_3C_6H_2$) in DMF/en solution. They adopt an almost perfectly T_d-symmetric structure with four discrete $[Ge_4]$ tetrahedra at the vertices of the supertetrahedron, with each of the six edges bridged by a single transition metal ion (Zn^{2+}/Cd^{2+}) in approximately square planar coordination (Figure 1).
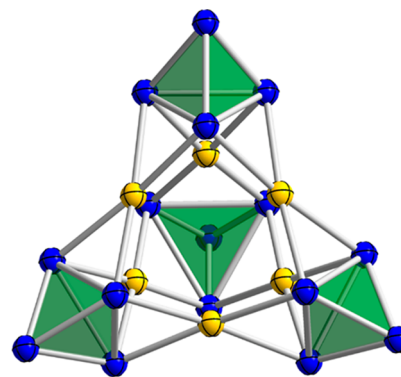

Figure 1. Crystal structure of the supertetrahedral clusters, $[M_6Ge_{16}]^{4-}$ (M = Zn, Cd), with Ge in blue and M in yellow.

The stability of these anions in solution was confirmed by electrospray mass spectrometry (ESI-MS) where intense signals for the parent ions and/or ion-pairs were observed. Continuous monitoring of the reaction solution via ESI-MS also provided important information on the assembly mechanism of the supertetrahedral $[M_6Ge_{16}]^{4-}$ clusters. A prominent peak assigned to $\{[K_3(2,2,2-crypt)][ZnGe_8]\}^-$ was observed in the initial stages of the reaction, which gradually reduced in intensity and was replaced by a species containing the target anion $\{[K(2,2,2-crypt)]_x[Zn_6Ge_{16}]\}^-$. This observation suggests that the $[ZnGe_8]$ unit may be a key intermediate in the formation of $[Zn_6Ge_{16}]^{4-}$. The electronic structure of the supertetrahedral clusters $[M_6Ge_{16}]^{4-}$ (M= Zn, Cd) was examined using density functional theory, followed by both adaptive natural density

partitioning (AdNDP) and analysis of the electron localization function (ELF). The calculations reveal that the occupied orbitals of the clusters can be decomposed into 12 3c-2e Ge−Ge−Ge σ bonds (three per Ge_4) and 12 3c-2e M−Ge−Ge σ bonds. The 3c-2e M−Ge−Ge σ bonding interactions between $[Ge_4]^{4-}$ and M^{2+} are indicative of substantial covalence rather than purely ionic interactions. The magnetic response properties of the supertetrahedra reveal that the 3c-2e M−Ge−Ge and Ge−Ge−Ge σ bonds have aromatic character and also that the tetrahedral Ge_4 units display spherical aromaticity, accounting for the stability of the $[M_6Ge_{16}]^{4-}$ clusters.

Among all the homonuclear deltahedral cluster anions $[E_x]^{q-}$ ($x = 4, 5, 9, 10$), the most common structural type is the trigonal bipyramid, $[E_5]^{2-}$, examples of which were structurally characterized more than 30 years ago.[39] Despite this, its reactivity remains relatively unexplored, perhaps because its *closo* deltahedral electronic structure renders it rather unreactive in solution. The *closo* electronic structure does, however, place a lone pair of electrons at each vertex, suggesting that these clusters should be able to act as potent nucleophiles without disrupting the skeletal electrons. As proof-of-concept, we have isolated the organometallic Zintl cluster $[Ge_5Ni_2(CO)_3]^{2-}$,[40] the first functionalized *closo*-$[E_5]^{2-}$ cluster. The anion was obtained from the reaction of the intermetallic precursor "$KGe_{1.67}$", from which trigonal bipyramidal $[Ge_5]^{2-}$ can be extracted, with the zerovalent Ni complex $Ni(CO)_2(PPh_3)_2$, and its structure can be viewed as a moderately distorted Ge_5 trigonal bipyramid coordinated to a neutral $[(\mu\text{-CO})(NiCO)_2]$ fragment (Figure 2). ESI-MS studies confirm the stability of the

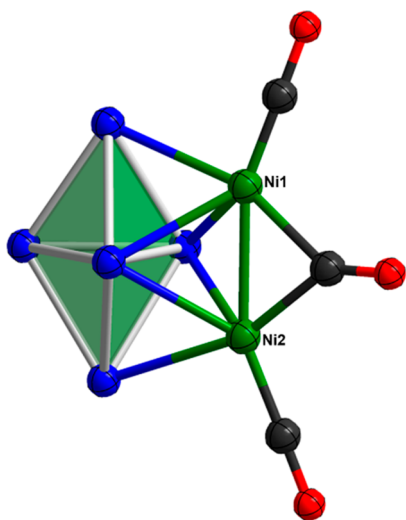**Figure 2.** Crystal structure of the cluster anion $[Ge_5Ni_2(CO)_3]^{2-}$, with Ge in blue, Ni in green, C in black, and O in red.

$[Ge_5Ni_2(CO)_3]^{2-}$ anion in solution in an ion-pair with $[K(2,2,2\text{-crypt})]^+$ but again offer some clues about possible formation pathways. Strong signals for both $[Ge_5]^-$ and anionic fragments of the transition metal reagent such as $[Ni_2(CO)_3(PPh_2)]^-$, $[Ni_2(CO)_2(PPh_2)]^-$, and $[Ni_2(CO)(PPh_2)]^-$ hint at a possible formation pathway involving capture of the *closo*-$[Ge_5]^{2-}$ anion by a nickel carbonyl fragment. The AdNDP method reveals that the four Ge_3 faces directed away from the $[(\mu\text{-CO})(NiCO)_2]$ unit remain largely unperturbed by the presence of the $Ni_2(CO)_3$ unit, while the remaining two Ge_3 triangles form two 4c−2e Ge−Ge−Ge−Ni σ delocalized bonds, in which approximately 81% of the contribution comes from the p-

orbitals of the three Ge atoms. Such a scenario is highly indicative of electron donation from the *closo* $[Ge_5]^{2-}$ cluster to the Ni dimer. Natural population analysis and calculated Wiberg bond indices also support the idea that a flow of electron density from the *closo*-$[Ge_5]^{2-}$ donor to the neutral $Ni_2(CO)_3$ fragment is the dominant bonding pathway, confirming our earlier assertion of the nucleophilicity of the *closo* $[E_5]^{2-}$ anions. The apparent simplicity of the bonding in this molecule hints at a rich Lewis-base chemistry for the *closo*-$[E_5]^{2-}$ anions.

During the course of our in-depth exploration of the reactivity of $[Ge_9]^{4-}$ with zerovalent d^{10} metals, we encountered a cluster assembled sandwich complex $\{(Ge_9)_2[\eta^6\text{-Ge}(PdPPh_3)_3]\}^{4-}$,[4] in which a planar $Ge@Pd_3$ unit is flanked by two Ge_9 cluster units. Sandwich complexes such as ferrocene $((\eta^5\text{-C}_5H_5)Fe(\eta^5\text{-C}_5H_5))$, bis-benzene chromium $((\eta^6\text{-C}_6H_6)Cr(\eta^6\text{-C}_6H_6))$, and uranocene $((\eta^8\text{-C}_8H_8)U(\eta^8\text{-C}_8H_8))$ are icons of organometallic chemistry, but sandwich-type complexes with a heterometallic cluster at the center had not previously been documented. This cluster was isolated from the reaction of K_4Ge_9 with $Pd(PPh_3)_4$ in the presence of a mild oxidizing agent, NC−HCPPh₃((triphenylphosphoranylidene)acetonitrile). The stability of the sandwich complex $\{(Ge_9)_2[\eta^6\text{-Ge}(PdPPh_3)_3]\}^{4-}$ even in solution was confirmed by the ESI-MS of the crystal dissolved in DMF, which shows strong signals assigned to the parent ion. The $\{(Ge_9)_2[\eta^6\text{-Ge}(PdPPh_3)_3]\}^{4-}$ anion can be viewed as a neutral heterometallic $Ge@(PdPPh_3)_3$ planar unit sandwiched between two *quasi*-D_{3h} tricapped trigonal prismatic $[Ge_9]^{2-}$ clusters in a μ^3-η^1:η^1:η^1-coordination mode (Figure 3a).
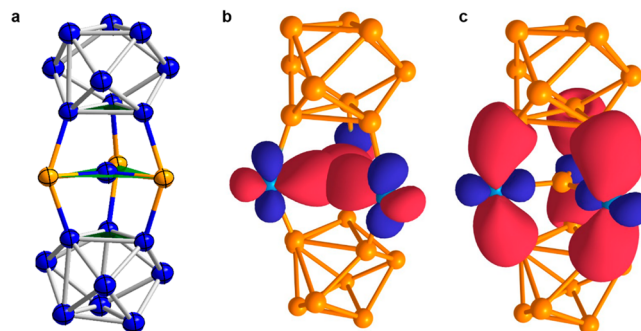

Figure 3. Crystal structure of the sandwich complex $\{(Ge_9)_2[\eta^6\text{-Ge}(PdPPh_3)_3]\}^{4-}$ with the $Pd(PPh_3)$ fragment denoted by a Pd atom (a), and selected results of the AdNDP analysis: T\three 2c-2e Pd−Ge σ-bonds (ON = 1.95 |e|) of $\{(Ge_9)_2[\eta^6\text{-Ge}(PdPH_3)_3]\}^{4-}$ (b), localized 2c−2e bonds of $\{(Ge_9)_2[\eta^6\text{-Ge}(PdPH_3)_3]\}^{4-}$, six 2c-2e Pd−Ge σ-bonds, ON = 1.95 |e| (c). Ge is blue, and Pd is gold.

The electronic structure, again explored using a combination of DFT and postanalysis using the AdNDP methodology, reveals that the $Ge@Pd_3$ unit is stabilized by three 2c-2e Pd−Ge σ-bonds (Figure 3b), while the bonding between the $Ge@Pd_3$ sheet and the two nona-germanide caps is supported by six 2c-2e Pd−Ge σ-bonds (Figure 3b) and two delocalized 4c-2e Ge−Ge−Ge−Ge σ-bonds. NBO analysis reveals that the central Ge atom and its bonded Pd atoms are approximately neutral. Very similar 4c-2e σ bonds were also identified in copper containing nanogermanide clusters such as $Cu[Ge_9\{P(NH_2)_2\}_3]$ and $Cu(NHC)[Ge_9\{P(NH_2)_2\}_3]^-$,[41] suggesting that they may be a general feature of zerovalent germanium chemistry, complementing the well-established stabilization of neutral Ge atoms by carbene ligands.[42] The magnetic response properties again reveal spherical aromaticity within the Ge_9 units, suggesting a

formulation as a neutral $Ge@(PdPPh_3)_3$ sheet sandwiched by two spherical aromatic nona-germanide clusters.

Another important objective in germanium Zintl-ion chemistry is the synthesis of endohedral $[M@Ge_{12}]^{q-}$ clusters. The heavier group IV analogues stannespherene $[Sn_{12}]^{2-}$ and plumbaspherene $[Pb_{12}]^{2-}$ are well-established species which have been isolated in naked form and also shown to be capable of encapsulating transition metal and f-block atoms while maintaining the icosahedral structure.[8,9] The $[Ge_{12}]^{2-}$ cluster itself was shown to have several near-degenerate minima, including the icosahedral structure,[43] while the most stable structures of endohedral $[M@Ge_{12}]^{q-}$ were predicted to be icosahedral, hexagonal prismatic, or completely nondeltahedral (D_{2d}-symmetric).[10] The latter has been realized in the form of $[Ru@Ge_{12}]^{3-}$, characterized by Goicoechea and co-workers in 2014,[17] but the other two types remain unknown. Research carried out in our lab yielded a fourth structural type, $[Co@Ge_{12}]^{3-}$ (Figure 4b) which is a highly distorted icosahedron with
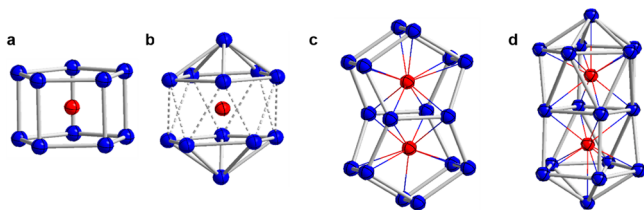

Figure 4. Crystal structures of $[Co@Ge_{10}]^{3-}$ (a), $[Co@Ge_{12}]^{3-}$ (b), α-$[Co_2@Ge_{16}]^{4-}$ (c), and β-$[Co_2@Ge_{16}]^{4-}$ (d). Ge is blue, and Co is red.

D_{5d} point symmetry.[44] The $[Co@Ge_{12}]^{3-}$ cluster was synthesized through the reaction of K_4Ge_9 with $[Co(I)Me-(PMe_3)_4]$ and was found to cocrystallize with the previously documented pentagonal prismatic anion $[Co@Ge_{10}]^{3-}$ (Figure 4a)[15] in the salt $[K(2,2,2\text{-crypt})]_3[CoGe_{12}]_{0.76}[CoGe_{10}]_{0.24}\cdot$ en.[44] The coexistence of the two cluster anions was confirmed by the ESI-MS of a DMF solution of the single crystals, where strong signals due to both $[CoGe_{10}]^-$ (m/z 784.25) and $[CoGe_{12}]^-$ (m/z 930.10) were observed. The $[Co@Ge_{12}]^{3-}$ anion is substantially distorted from the icosahedral limit, with long Ge–Ge distances (av. 2.902 Å) between the two capped pentagonal Ge_6 units and rather shorter bonds within the Ge_6 units (av. 2.640 (8) Å). The dramatic elongation of the icosahedron can be traced to a strong second-order Jahn–Teller distortion, but an alternative limiting view is as a sandwich complex of cobalt with two Ge_6 ligands. However, all Ge–Ge distances remain within the range established by known Ge_9 clusters (2.5–2.9 Å), although they are strikingly longer than typical Ge–Ge single-bonds (2.40–2.44 Å). The Co–Ge_6 contacts (to the pentagonal Ge_6 ligands) are also longer than those in the D_{5h} pentagonal prism $[Co@Ge_{10}]^{3-}$. The elongation of the Ge–Ge and Co–Ge bonds is reflected in the AdNDP analysis, which reveals that each $CoGe_6$ unit contains five 7c-2e delocalized bonds while the Ge_5–Co–Ge_5 pentagonal prism contains three 11c-2e delocalized bonds. Further electronic structure analysis of I_h-$[Ge_{12}]^{2-}$ and its encapsulated derivatives $[M@Ge_{12}]^{3-}$ (M = Co, Rh, Ir, and Mt) reveals that the cage size of the $[Ge_{12}]^{2-}$ anion, with a diameter of 5.2 Å, is too small to accommodate even the Co atom (5.65 Å), and the even larger endohedral metal atoms of the second, third, and fourth transition series amplify the distortion toward a genuinely sandwich-like structure (Figure 4b).

The crystallographic data for $[Co@Ge_{10}]^{3-}$ and $[Co@Ge_{12}]^{3-}$ can usefully be compared with the structural chemistry of the intermetalloid cluster $[Co_2@Ge_{16}]^{4-}$, which was synthesized from the reaction of K_4Ge_9 with $[\{(ArN)_2C^tBu\}\text{-}Co(I)(\eta^6\text{-toluene})]$ (Ar = 2,6-diisopropylphenyl). The very different outcomes of the two reactions suggest that the ligands can play a defining role in the path of reactions that generate Zintl clusters.[45] The stability of the $Co_2@Ge_{16}$ unit in solution was again confirmed by ESI-MS studies of the reaction solution which showed the presence of the oxidized parent ion $[Co_2@Ge_{16}]^-$ and its $[K(2,2,2\text{-crypt})]^+$ complexed ion-pair $\{[K(2,2,2\text{-crypt})][Co_2@Ge_{16}]\}^-$. The $[Co_2@Ge_{16}]^{4-}$ cluster crystallizes as a mixture of two quite distinct isomeric forms, a dominant D_{2h}-symmetric (α) form (Figure 4c) along with a minor C_{2h}-symmetric (β) component (Figure 4d) in a ratio of 1:9. The α form features 3-connected Ge atoms, much like $[Co@Ge_{10}]^{3-}$, and represents the largest group 14 nondeltahedral homoatomic cluster containing more than one interstitial metal atom. The β isomer, in contrast, is quasi-deltahedral and in that sense bears closer resemblance to the D_{5d}-symmetric $[Co@Ge_{12}]^{3-}$ anion. Thus, the delicate balance between deltahedral and 3-connected structural types seems to be a common feature of Co/Ge chemistry, irrespective of the dimensions of the cluster. The DFT-computed potential energy surface confirms that the two isomers are almost degenerate. Direct Co–Co interactions are absent in both isomers, but the Ge–Ge contacts in the α isomer are significantly shorter than those in the β isomer, reflecting their very different electronic structure. Analysis of the computed density using the AdNDP method indicates that the skeleton of the α isomer is dominated by localized bonding, although there are also two Co–Ge–Ge–Co 4c-2e π bonds and one 6c-2e Co–Ge_4–Co σ-bond, in which the contribution of the two Co atoms is very low. In contrast, the β isomer contains only multicenter delocalized bonds, including five 7c-2e delocalized σ-bonds in the Co-centered pentagonal Ge_6 units and one 6c-2e σ-bond linking the two Co atoms to the central Ge_4 square. The two isomers have the same number of bonds between the pentagonal Ge_6 "hats" and the central Ge_4 plane, but the α isomer has more local bonds in the Ge_6 moiety than its β counterpart (7 vs 5), suggesting that the α isomer is more electron rich.

3. TIN-BASED INTERMETALLOID CLUSTERS AND THEIR APPLICATIONS IN BOTTOM-UP SYNTHESIS

The empty $[E_9]^{q-}$ cages (E = Ge, Sn, q = 3, 4) are well-known, as are the corresponding endohedral clusters $[M@E_9]^{q-}$ (M = Cu, Ni) and also endohedral clusters with capping ligated heteroatoms such as $[Ni@E_9\text{-}Ni(CO)]^{3-}$, $[Ni@Ge_9\text{-}Ni\text{-}(en)]^{3-}$, and $[Pt@Sn_9\text{-}Pt(PPh_3)]^{2-}$.[22,23] The latter are usually obtained from one-pot reactions using the $[E_9]^{4-}$ anions as starting materials. Only in the past decade has it become apparent that the centered $[M@E_9]^{q-}$ clusters share the rich chemistry shown by the parent $[E_9]^{q-}$ cages, a point most elegantly illustrated by Sevov's isolation and characterization of the $[Ni@Sn_9]^{3-}$ and $[Ni@Sn_9]^{4-}$ redox pair[46] which mirrors the electron transfer chemistry of the $[Sn_9]^{3-}/[Sn_9]^{4-}$ couple. It was against this background that we first undertook a systematic study of the reactivity of the Co centered deltahedral cluster $[Co@Sn_9]^{4-}$, which can be extracted from a ternary solid-state phase "$K_5Co_3Sn_9$" in high yield and proves to be a good precursor for reactions with various organometallic reagents. Four ternary functionalized cluster anions of general formula $[Co@Sn_9\text{-}ML]^{3-}$ (ML= Ni(CO), Ni(C_2H_4), Pt(PPh_3), and
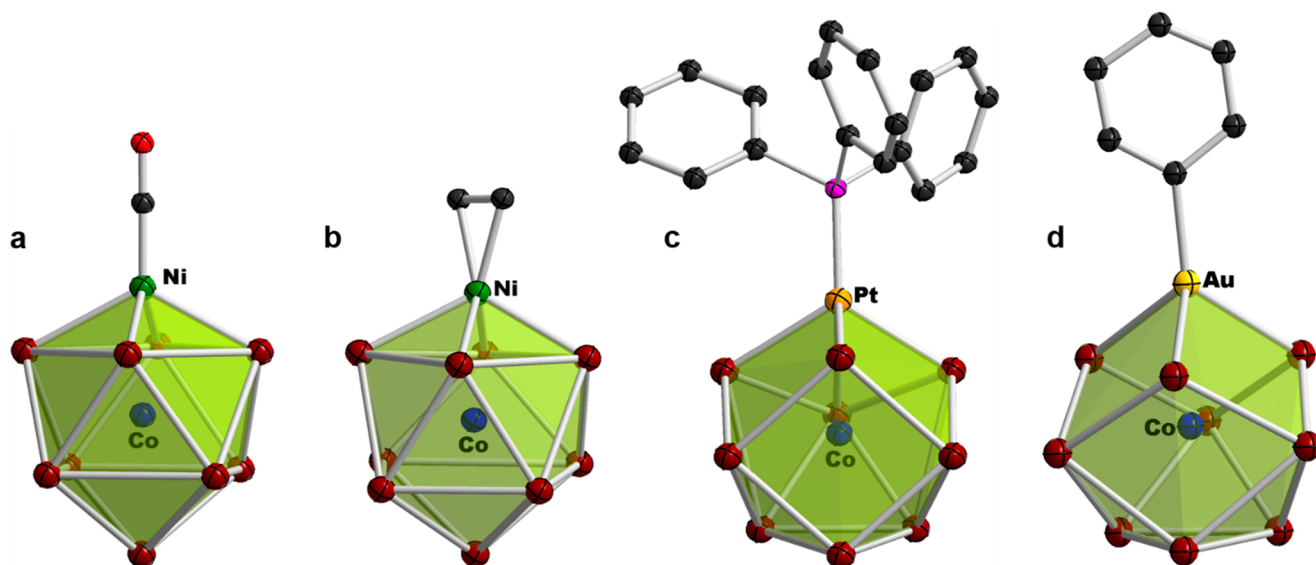
Figure 5. Crystal structures of $[Co@Sn_9-Ni(CO)]^{3-}$ (a), $[Co@Sn_9-Ni(C_2H_4)]^{3-}$ (b), $[Co@Sn_9-Pt(PPh_3)]^{3-}$ (c), and $[Co@Sn_9-Au(Ph)]^{3-}$ (d). Sn is dark red, Ni is green, Pt is brown, Au is gold, C is black, O is red, and P is purple.
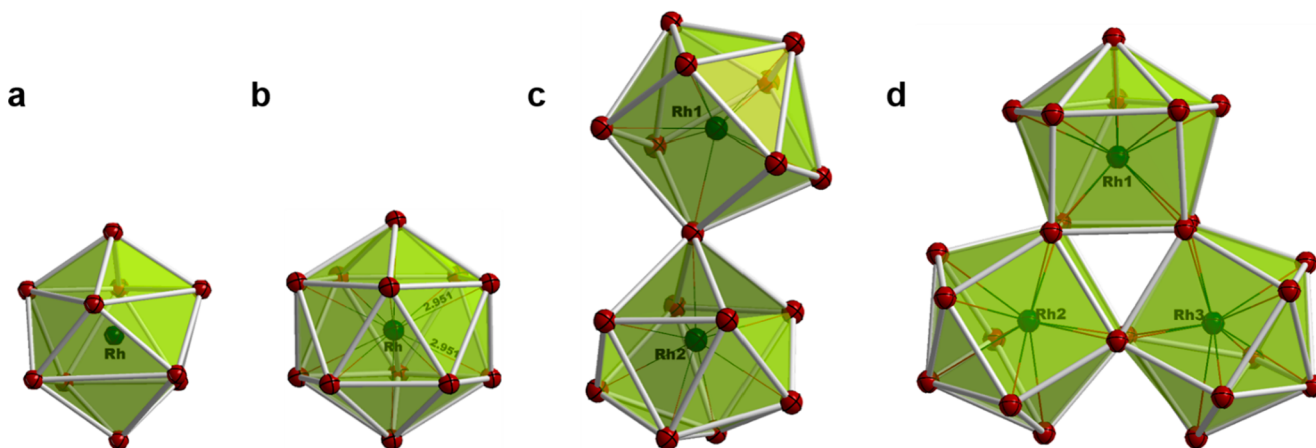

Figure 6. Crystal structures of the $[Rh_x@Sn_y]^{q-}$ intermetalloids: $[Rh@Sn_{10}]^{3-}$ (a), $[Rh@Sn_{12}]^{3-}$ (b), $[Rh_2@Sn_{17}]^{6-}$ (c), and $[Rh_3@Sn_{24}]^{5-}$ (d), with Sn in dark-red and Rh in green.

Au(Ph)) have been generated from the reaction of $[Co@Sn_9]^{4-}$ with the corresponding transition metal compounds, Ni-$(PPh_3)_2(CO)_2$, $Ni(COD)_2$, $Pt(PPh_3)_4$, and $Au(PPh_3)Ph$, respectively.[47] The M−Co@Sn$_9$ cluster is an approximately C_{4v} symmetric monocapped square antiprism in the first two (Figure 5a and 5b), while it is a *pseudo-C_{3v}* symmetric tricapped trigonal prismatic structure for the other two clusters (Figure 5c and 5d). All four Co-centered clusters are stable in solution, as confirmed by intense ESI-MS signals for the parent ions $[Co@Sn_9-ML]^-$ and their ion-pairs $[K(2,2,2\text{-crypt})_x(Co@Sn_9-ML)]^-$. Geometry optimizations of $[Co@Sn_9-Ni(CO)]^{3-}$ and $[Co@Sn_9\text{-}Au(Ph)]^{3-}$ anions using DFT indicate that there is very little difference between the two structural forms ($\Delta E = E(C_{4v}) - E(C_{3v}) = -0.27$ eV for $[Co@Sn_9-Ni(CO)]^{3-}$ and $+0.31$ eV for $[Co@Sn_9-Au(Ph)]^{3-}$), but the relative energies are consistent with the adoption of C_{4v} and C_{3v} structures, respectively. Significant Co-ML σ interactions emerge in all four anions. The isolation and characterization of this family of ternary functionalized cluster anions $[Co@Sn_9-ML]^{3-}$ hold out promise of a rich chemistry based on the reactivity of the $[Co@Sn_9]^{4-}$ anion.

The largest known tin-based intermetalloid cluster is the multiply shell "Matryoshka" anion $[Sn@Cu_{12}@Sn_{20}]^{12-}$, characterized in salt-like intermetallic $A_{12}Cu_{12}Sn_{21}$ (A = Na, K).[48] Solution-phase synthetic routes, in contrast, appeared until recently to be limited to rather small clusters such as phase $[Pd_2@Sn_{18}]^{4-}$,[12] and clusters with more than 18 tetrel atoms or more than three interstitial transition metal ions had never been isolated in this way. This *status quo* held until very recently, when we characterized two large intermetalloid cluster anions, $[Rh_3@Sn_{24}]^{5-}$[11] and $[Cu_4@E_{18}]^{4-}$ (E = Sn, Pb) where a Cu_4 rhombus is embedded in an 18-vertex cluster.[3] The triply fused stannide $[Rh_3@Sn_{24}]^{5-}$, the largest known endohedral Group 14 Zintl anion, was isolated from reaction of K_4Sn_9 with $[Rh(COE)_2Cl]_2$ (COE = cyclooctene) or, alternatively, via thermal fragmentation/rearrangement of the $[Rh@Sn_{10}]^{3-}$ anion in DMF solution. We note in this context that DMF has found extensive use in Zintl-ion solution chemistry for thermal deligation and oxidation reactions that generate large clusters.[49] Three further Sn−Rh intermetalloid clusters, $[Rh@Sn_{10}]^{6-}$ and the I_h- and D_{3d}-symmetric isomers of $[Rh@Sn_{12}]^{3-}$ and $[Rh_2@Sn_{17}]^{3-}$, have also been synthesized and characterized through subtle

modifications of the same reaction between K_4Sn_9 and $[Rh(COE)_2Cl]_2$.[11] The stability of these endohedral clusters has been confirmed by ESI-MS. Although the crystal of $[Rh@Sn_{10}]^{3-}$ suffered from serious positional disorder, its oxidation state and bicapped square antiprismatic structure, which is distorted significantly from the ideal D_{4d} symmetry, were established with reasonable certainty (Figure 6a). The icosahedral cluster $[Rh@Sn_{12}]^{3-}$, which crystallizes alongside $[Rh@Sn_{10}]^{3-}$, contains individual I_h- and D_{3d}-symmetric isomers in the unit cell. An analysis of the potential energy surface shows that I_h- and D_{3d}-$[Rh@Sn_{12}]^{3-}$ (Figure 6b) are approximately iso-energetic, suggesting again that the structural variance results from crystal packing. A similar flat surface prevails in the $[Rh@Sn_{10}]^{3-}$ cluster, where the experimentally observed bicapped square antiprismatic structure (D_{4d}-symmetry) lies only 0.16 eV higher than the global minimum, a C_{2v}-symmetric structure. The $[Rh_2@Sn_{17}]^{6-}$ anion (Figure 6c) was obtained from the mother liquor depleted of both $[Rh@Sn_{10}]^{3-}$ and $[Rh@Sn_{12}]^{3-}$ crystals. The hexa-anion is surrounded by three tightly bound K^+ cations to form $[K_3(Rh_2@Sn_{17})]^{3-}$, with K–Sn contacts in the range of 3.5980(11)–3.7865(13) Å. The $[Rh_2@Sn_{17}]^{6-}$ anion can be viewed as a coalescence of two $[Rh@Sn_9]$ units via a shared Sn vertex. It is structurally similar to D_{2d}-symmetric $[M_2@Sn_{17}]^{4-}$ (M = Ni, Pt)[13,14] but with a pronounced bending at the shared Sn atom (Rh–Sn–Rh = 163.9°). Structural optimizations on $[Rh_2@Sn_{17}]^{6-}$ and $[K_3(Rh_2@Sn_{17})]^{3-}$ demonstrated that the global minimum of the former is a perfectly D_{2d} structure with a linear Rh–Sn–Rh unit, isostructural with the known and isoelectronic $[Ni_2@Sn_{17}]^{4-}$ compound. The pronounced Rh–Sn–Rh bending is therefore a consequence of the presence of three tightly bonded K^+ cations which necessarily breaks the 2-fold rotational symmetry of the D_{2d}-symmetric parent. The $[Rh_3@Sn_{24}]^{5-}$ anion is C_{3v}-symmetric and can be viewed as a perfect Sn_6 triangular prism with each of its three square-faces capped by a Rh-centered Sn capped pentagonal $RhSn_6$ unit or, alternatively, as a fusion of three $[Rh@Sn_{10}]$ units around a Sn_6 triangular prism (Figure 6d). The yield of the $[Rh_3@Sn_{24}]^{5-}$ anion is somewhat higher from the thermal fragmentation/rearrangement of the preformed $[Rh@Sn_{10}]^{3-}$ anion than it is from the aforementioned reaction of K_4Sn_9 with $[Rh(COE)_2Cl]_2$, suggesting that heteroatomic fragments such as $[Rh_xSn_y]^{q-}$ may be intermediates in the growth of larger $[Rh_x@Sn_y]^{q-}$ intermetalloid clusters. In particular, the $[RhSn_8]^{q-}$ fragment that is ubiquitous in all our ESI-MS studies on this system is a likely candidate although, as is the case with other reactions described in this review, the precise cluster growth mechanism remains unclear.

A further significant development in solution-based deltahedral Zintl anion chemistry came with the isolation and characterization of two intermetalloid clusters $[Cu_4@E_{18}]^{4-}$ (E = Sn, Pb), which represent the first examples of an M_4 cluster inside a continuous E_{18} tetrel cage (Figure 7).[3] Prior to this report, intermetalloid clusters of group 14 elements were limited to only one or two insertion atoms, with the single exception being $[Ni_3@Ge_{18}]^{4-}$ which has three.[10] The two $[Cu_4@E_{18}]^{4-}$ anions (E = Sn, Pb) are prepared by the reaction of K_4E_9 with $Cu_4Mes_4(THT)_2$ and are isostructural, with D_{2h} point symmetry. Their stability in solution were corroborated by the presence of both the parent ion and the ion-pair with $[K(2,2,2$-crypt$)_x]^+$ in the ESI-MS in each case. The $[E_{18}]$ cage of $[Cu_4@E_{18}]^{4-}$ can be viewed as two icosahedral $[E_{12}]^{2-}$ molecules fused by the removal of two E_3 triangular faces (Figure 8). The Cu
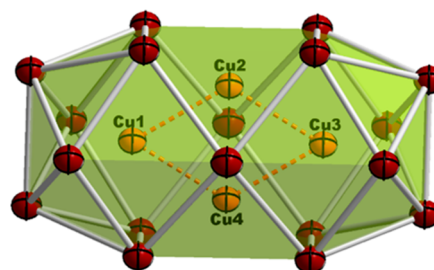

Figure 7. Crystal structure of $[Cu_4@Sn_{18}]^{4-}$, where Sn is dark red and Cu is brown.
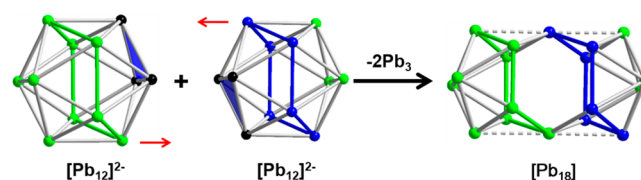

Figure 8. Structural relationship between $[Cu_4@Pb_{18}]^{4-}$ and $[Pb_{12}]^{2-}$.

atoms in the $[Cu_4@E_{18}]^{4-}$ clusters are of two distinct types: those at the foci of the E_{10} units are 10-coordinate while the Cu2 atoms are in approximate trigonal prismatic coordination. An analysis of the electronic structure suggests that the role of these latter two Cu ions is primarily charge balance rather than structural, because the optimized structure of the $[Cu_2@E_{18}]^{6-}$ anions where these Cu ions are removed is almost identical to the parent clusters. The relatively loose association of these Cu2 ions with the cluster offers the intriguing possibility that they may play a role in cluster growth by acting as a template for fusion before carrying away excess electron density: we note in this context that the formation of Cu mirrors is a common side-reaction in many of the reactions described here. The $[Cu_4@Sn_{18}]^{4-}$ cluster differs from the Matryoshka cluster $[Sn@Cu_{12}@Sn_{20}]^{12-}$ only in the Cu:Sn ratio, and both can be viewed in some sense as steps toward a bronze-like alloy. A comparison of the electronic structures of the two clusters confirms the close similarity between the two (Figure 9).

4. LEAD CLUSTERS WITH PRECIOUS METAL CORES

Compared to the light analogues, $[Ge_9]^{4-}$ and $[Sn_9]^{4-}$, described in the previous paragraphs, derivatives of the $[Pb_9]^{4-}$ precursor are notably less common, probably as a result of the higher activity of $[Pb_9]^{4-}$ compared to either $[Ge_9]^{4-}$ or $[Sn_9]^{4-}$. In fact, the Zintl-ion chemistry of lead is dominated by endohedral icosahedral clusters of general formula $[M@Pb_{12}]^{q-}$, and several different transition metal atoms (Mn, Ni, Pd, Pt) have been successfully embedded inside the plumbaspherene $[Pb_{12}]^{2-}$ cage via reactions of $[Pb_9]^{4-}$ with appropriate low-valent transition metal complexes. In an extension to this chemistry, we have recently isolated the $[Au@Pb_{12}]^{3-}$ anion from the reaction of K_4Pb_9 with $Au(PPh_3)Ph$ in pyridine solution,[50] the first example of this class containing a coinage metal. This cluster is very strikingly distorted from perfectly I_h icosahedral geometry and instead adopts an approximately D_{3d}-symmetric structure. The $[Au@Pb_{12}]^{3-}$ anion has two more valence electrons than the perfectly icosahedral clusters $[M@Pb_{12}]^{2-}$ (M = Ni, Pd, Pt)[8] and $[M@Pb_{12}]^{3-}$ (M = Co, Rh, Ir)[9] where all M atoms have a d^{10} configuration and four more valence electrons than that for formally d^8 $[Mn@Pb_{12}]^{3-}$, which is also strongly distorted, in that case along a D_{2h}-symmetric
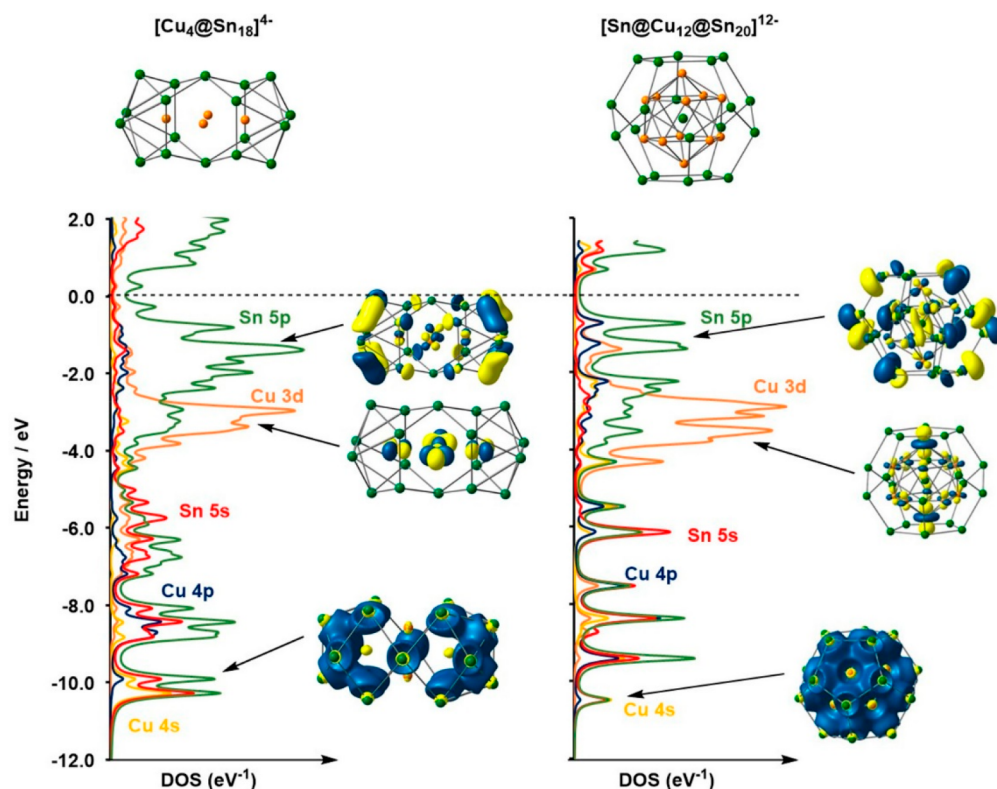
Figure 9. Comparison of the density of states for $[Cu_4@Sn_{18}]^{4-}$ and $[Sn@Cu_{12}@Sn_{20}]^{12-}$. Eigenvalues are broadened with a Lorentzian line shape with full width at half-maximum of 0.1 eV. Adapted with permission from ref 3. Copyright (2020) ACS.
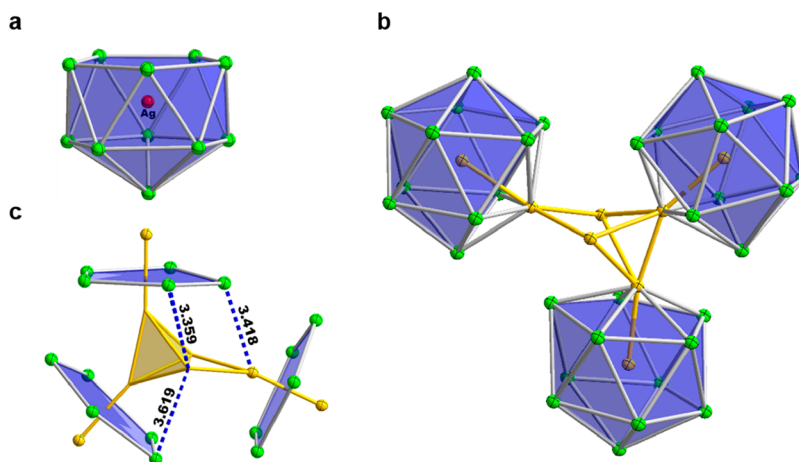

Figure 10. Crystal structures of $[Ag@Pb_{11}]^{3-}$ (a), $[Au_8Pb_{33}]^{6-}$ (b), and selected secondary π-type Pb⋯Au interactions in the $[Au_8Pb_{33}]^{6-}$ anion, with the secondary Pb⋯Au contacts labeled (c).

coordinate.[51] Intrigued by the interesting electronic structure of $[Au@Pb_{12}]^{3-}$, we have extended our study of the reactivity of coinage metal complexes with $[Pb_9]^{4-}$ and developed the synthesis of a series of clusters, $[Ag@Pb_{11}]^{3-}$, $[Au_8Pb_{33}]^{6-}$, and $[Au_{12}Pb_{44}]^{8-}$,[1] from the reactions of $[Pb_9]^{4-}$ with $(AgMes)_4$ or $Au(Mes)PPh_3$ (Mes = 1,3,5-trimethylbenzene) in ethylenediamine or pyridine solution. The $[Ag@Pb_{11}]^{3-}$ cluster represents the first example of a *nido* icosahedron containing an endohedral atom and is also the first binary Ag−Pb Zintl anion (Figure 10a). We note here that Eichhorn and co-workers have very recently reported two $[Ru(Cp^*)]^+$ functionalized *nido*-icosahedral Zintl anions $[Pb_{11}(\eta^5\text{-RuCp*})]^{3-}$ and $[Cu@Pb_{11}(\eta^5\text{-RuCp*})]^{2-}$, the latter containing an endohedral Cu^+ ion.[52] $[Au_8Pb_{33}]^{6-}$ and

$[Au_{12}Pb_{44}]^{8-}$ contain three and four Au-centered *nido* icosahedral $[Au@Pb_{11}]$ units, respectively, and each of these units is isostructural with the $[Ag@Pb_{11}]^{3-}$ cluster described above. In this sense, $[Au_8Pb_{33}]^{6-}$ could be considered, at least in a structural sense, as three *nido* icosahedral $[Au@Pb_{11}]^{3-}$ units with their open Pb_5 faces linked by a $[Au_5]^{3+}$ core (Figure 10b), while $[Au_{12}Pb_{44}]^{8-}$ can be viewed in an analogous manner as four $[Au@Pb_{11}]^{3-}$ units bound to four corners of an $[Au_8]^{4+}$ cube (Figure 11). However, the absence of the signals for large gold clusters such as $[Au_5]$ and $[Au_8]$ in the ESI-MS suggests that this perspective is perhaps only a formalism and does not necessarily reflect the growth pathways that lead to these large clusters. We do, however, detect signals for $[Au@Pb_{11}]^-$ and
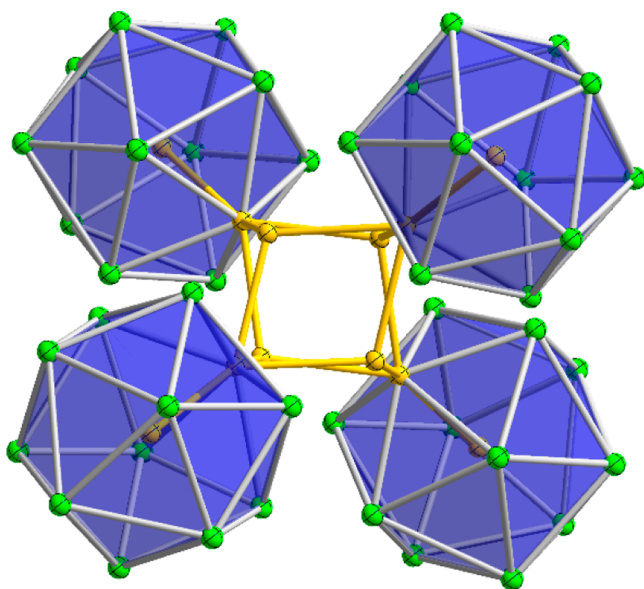
Figure 11. Crystal structure of the $[Au_{12}Pb_{44}]^{8-}$ anion, where Pb is green and Au is gold.

$[Au_2Pb_{11}]^-$ in the ESI-MS in all reactions but no analogous $[Ag_2Pb_{11}]^-$ signal for the Ag-based chemistry that generates only $[Ag@Pb_{11}]^{3-}$. Based on this observation, we believe that the $[Au_2Pb_{11}]^-$ moiety may be an important intermediate in the formation of the large Au–Pb clusters, while the relative instability of $[Ag_2Pb_{11}]^-$ accounts for the absence of Ag analogues of the $[Au_8Pb_{33}]^{6-}$ and $[Au_{12}Pb_{44}]^{8-}$ anions.

DFT suggests that the intermediate cluster anion $[Au@AuPb_{11}]^{2-}$ is energetically accessible, while the binding of Ag^+ to the open Pb_5 face in $[Ag@AgPb_{11}]^{2-}$ is considerably weaker. A cluster growth mechanism that is consistent with these observations invokes the aggregation of the Au-capped Au centered icosahedral cluster $[Au@AuPb_{11}]^{2-}$ with excess Au^+ derived from $Au(Mes)PPh_3$, e.g. $3[Au_2Pb_{11}]^{2-} + 2Au^+$ for the former and $4[Au_2Pb_{11}]^{2-} + 4Au^+$ for the latter (Figure 12). In this sense, other Au/Pb clusters, assembled from the aggregation

of the $[Au_2Pb_{11}]^{2-}$ subunits with Au^+ ions, may also be accessible. The electronic structure of these clusters reveals the importance of secondary π-type interactions between the open Pb_5 face of the *nido*-$[Au@Pb_{11}]^{3-}$ and remote Au atoms (i.e., those not directly bound to the open face) in stabilizing the large Au–Pb cluster. The successful synthesis and characterization of these two large Au–Pb clusters, $[Au_8Pb_{33}]^{6-}$ and $[Au_{12}Pb_{44}]^{8-}$, represents a significant expansion of the range of Pb-based Zintl-ion chemistry.

5. CONCLUSION AND OUTLOOK

In this Account we have highlighted a number of recent advances in synthetic methodology that have allowed us to extend the range of known Zintl-ion chemistry. The reactions between Zintl phases A_xE_y, where both covalent and ionic contributions to bonding are important, and organometallic complexes which are dominated by covalent bonding lead to substantial rearrangements, and the resulting metal-doped Zintl anions often exhibit unique structures and bonding patterns. Moreover, seemingly subtle changes to the steric and electronic properties of the ligand and even reaction conditions (e.g., temperature, solvent or cation-sequestering agent, etc.) provide a powerful tool for manipulating the product distribution. This not only gives access to new clusters but also provides a window into the mechanism of cluster growth, as exemplified by our studies of the formation of $[Rh_3@Sn_{24}]^{5-}$ from $[Sn_9]^{4-}$ via (possibly) intermediate Rh_1- and Rh_2-containing clusters.

The electronic structure of these clusters continues to present challenges to theory. The structure and stability of the majority of the clusters can, on an individual basis, be postrationalized in terms of existing paradigms of cluster bonding (Wade-Mingos rules, spherical aromaticity, and superaromaticity, all of which have been used in aspects of this Account). As a result of these studies we have been able to identify previously unsuspected features of the bonding such as the secondary Pb···Au interactions in $[Au_8Pb_{33}]^{6-}$ and $[Au_{12}Pb_{44}]^{8-}$ that highlight the limitations of simple Lewis-type structures based on localized 2c-2e bonds. It is very clear, however, that we do not yet have an overarching predictive model of growth,

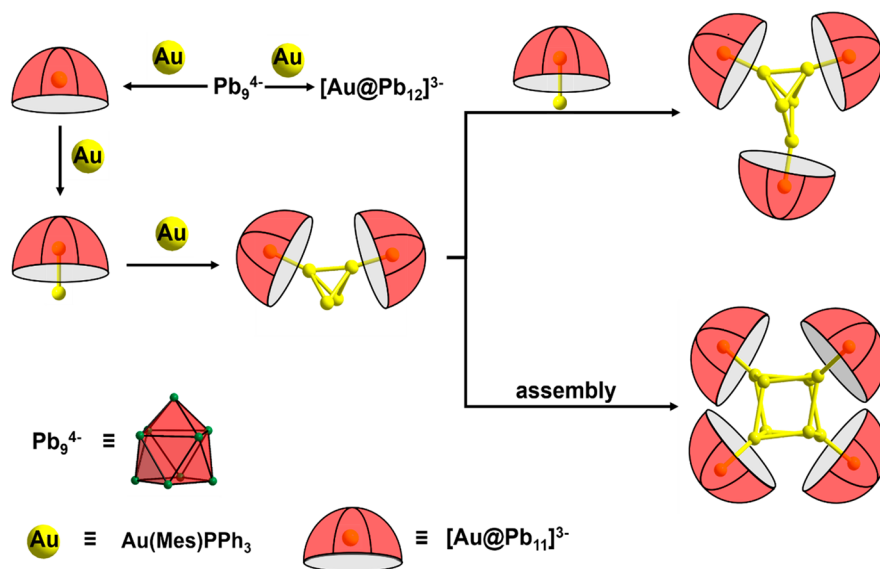**Figure 12.** Possible pathways leading to cluster growth. Coalescence of smaller component clusters leads to the assembly of $[Au_8Pb_{33}]^{6-}$ and $[Au_{12}Pb_{44}]^{8-}$. The $[Au@AuPb_{11}]$, $[Au_8Pb_{33}]$, and $[Au_{12}Pb_{44}]$ clusters have all been observed, by either X-ray crystallography or ESI-MS.

composition, and structure that would enable us to identify plausible targets or indeed rational routes to their synthesis. Beyond the well-documented limitations of density functional theory, there are technical issues associated with the large prevailing negative charges and the resulting large lattice. It is possible, therefore, that the isolation of a compound in the solid-state may reflect the balance between solvation and lattice enthalpy as much as it reflects the intrinsic stability of the cluster anion itself. The nature of the ESI-MS experiment means that the clusters observed are typically monoanionic, so although they share the same composition as many of the isolated clusters, the link between the two experiments is indirect. We anticipate that the next frontier in Zintl-ion chemistry will therefore be to establish a more nuanced understanding of structure−stability relationships that will open up routes to the rational synthesis of larger clusters of well-defined composition and structure. These clusters have already shown promise as precursors with important applications in materials chemistry: they have proven to be viable precursors for intermetallic nanoparticles[53] which show promising catalytic activity. Early applications of this strategy have shown great promise in the selective catalytic reduction of CO_2 by a CeO_2-dispersed isolated Ru catalyst obtained from the $[Ru@Sn_9]^{6-}$ cluster.[54] Goicoechea and co-workers have also highlighted applications in homogeneous catalysis, specifically the catalytic hydrogenation of cyclic alkenes using an $[\eta^4\text{-}Ge_9(Hyp)_3]Rh(COD)$ cluster.[55] The Zintl cluster $[Bi_9\{Ru(COD)\}_2]^{3-}$ has also proven capable of activating small molecules such as O_2 to generate $[Bi_9\{Ru(COD)\}_2O_2]^-$.[56] These exciting new results suggest that Zintl-ion chemistry will continue to generate surprises that will challenge our understanding of structure and bonding and also open up new avenues of synthetic and catalytic chemistry.

■ AUTHOR INFORMATION

Corresponding Author

Zhong-Ming Sun − *Tianjin Key Lab of Rare Earth Materials and Applications, State Key Laboratory of Elemento-Organic Chemistry, School of Materials Science and Engineering, Nankai University, Tianjin 300350, China;* ⊙ orcid.org/0000-0003-2894-6327; Email: sunlab@nankai.edu.cn

Authors

Yi Wang − *Tianjin Key Lab of Rare Earth Materials and Applications, State Key Laboratory of Elemento-Organic Chemistry, School of Materials Science and Engineering, Nankai University, Tianjin 300350, China*

John E. McGrady − *Department of Chemistry, University of Oxford, Oxford OX1 3QR, U.K.;* ⊙ orcid.org/0000-0002-8991-1921

Complete contact information is available at:
https://pubs.acs.org/10.1021/acs.accounts.0c00876

Notes

The authors declare no competing financial interest.

Biographies

Yi Wang received his B.Sc. (2010) from Zhengzhou University and his Ph.D. (2015) in organic chemistry from Fujian Institute of Research on the Structure of Matter, Chinese Academy of Sciences (CAS). He then spent four and a half years as a postdoc in USA with Prof. Bryan W. Eichhorn at University of Maryland, College Park. His research interests include the experimental synthesis of new Zintl clusters. He is currently working as a visiting research assistant professor at Nankai University.

John E. McGrady is Professor of Computational Inorganic Chemistry at the University of Oxford. He studied chemistry at St Catherine's College, Oxford, and then moved to Australia to study for a doctorate at the Australian National University. In 1997, he was appointed as a lecturer at the University of York, before moving to the University of Glasgow as a WestCHEM Professor in 2006. In 2009 he returned to the University of Oxford, becoming a fellow at New College. His research interests relate to the electronic structure of inorganic systems, metal cluster complexes, and metal−metal bonds

Zhong-Ming Sun received his B.Sc. (2001) from Wuhan University and his Ph.D. (2006) in Physical Chemistry from Fujian Institute of Research on the Structure of Matter, CAS. After a four-year postdoctoral stay at Washington State University/Pacific Northwest National Laboratory and North Dakota State University, he accepted an appointment as a full professor at Changchun Institute of Applied Chemistry, CAS, and worked there until 2018. He then relocated his lab to Nankai University, becoming a faculty member in the school of materials science and engeering. His main research interests include the synthesis of new metal clusters, metal−metal bonds, and cluster-assembled materials.

■ ABBREVIATIONS

AdNDP, adaptive natural density partitioning; 2,2,2-crypt, 4,7,13,16,21,24-hexaoxa-1,10-diazabicyclo[8.8.8]hexacosane; DFT, density functional theory; NBO, natural bond orbital; NICS, nucleus independent chemical shift; ESI-MS, electro-spray mass specscopy; Mes, mesitylene; Hyp, tris-(trimethylsilyl)silane; Cp*, pentamethylcyclopentadienyl

■ REFERENCES

(1) Shu, C.-C.; Morgan, H. W. T.; Qiao, L.; McGrady, J. E.; Sun, Z.-M. A family of lead clusters with precious metal cores. *Nat. Commun.* **2020**, *11*, 3477.

(2) Xu, H. L.; Popov, I. A.; Tkachenko, N. V.; Wang, Z. C.; Muñoz-Castro, A.; Boldyrev, A. I.; Sun, Z. M. σ-aromaticity-induced stabilization of heterometallic supertetrahedral clusters $[Zn_6Ge_{16}]^{4-}$ and $[Cd_6Ge_{16}]^{4-}$. *Angew. Chem., Int. Ed.* **2020**, *59*, 17286−17290.

(3) Qiao, L.; Zhang, C.; Shu, C.-C.; Morgan, H. W. T; McGrady, J. E.; Sun, Z.-M. $[Cu_4@E_{18}]^{4-}$ (E= Sn, Pb): Fused derivatives of endohedral stannaspherene and plumbaspherene. *J. Am. Chem. Soc.* **2020**, *142*, 13288−13293.

(4) Xu, H.-L.; Tkachenko, N. V.; Wang, Z.-C.; Chen, W.-X.; Qiao, L.; Muñoz-Castro, A.; Boldyrev, A. I.; Sun, Z.-M. A sandwich-type cluster containing $Ge@Pd_3$ planar fragment flanked by aromatic non-agermanide caps. *Nat. Commun.* **2020**, *11*, 5286.

(5) Zintl, E.; Harder, A. Metals and alloys. II. Polyplumbides, polystannides and their transition into metal phases. *Z. Phys. Chem., Abt. A* **1931**, *154*, 47−91.

(6) Queneau, V.; Sevov, S. C. Ge: A Deltahedral Zintl Ion Now Made in the Solid-State. *Angew. Chem., Int. Ed. Engl.* **1997**, *36*, 1754−1756.

(7) Eichhorn, B. W.; Haushalter, R. C.; Pennington, W. T. Synthesis and structure of closo-$Sn_9Cr(CO)_3^{4-}$: The first member in a new class of polyhedral clusters. *J. Am. Chem. Soc.* **1988**, *110*, 8704−8706.

(8) Esenturk, E. N.; Fettinger, J.; Eichhorn, B. The Pb_{12}^{2-} and Pb_{10}^{2-} Zintl ions and the $M@Pb_{12}^{2-}$ and $M@Pb_{10}^{2-}$ cluster series where M= Ni, Pd, Pt. *J. Am. Chem. Soc.* **2006**, *128*, 9178−9186.

(9) Li, A.-M.; Wang, Y.; Downing, D. O.; Chen, F.; Zavalij, P. Y.; Muñoz-Castro, A.; Eichhorn, B. Endohedral Plumbaspherenes of the

Group 9 Metals: Synthesis, Structure and Properties of the [M@Pb$_{12}$]$^{3-}$ (M= Co, Rh, Ir) Ions. *Chem. - Eur. J.* **2020**, *26*, 5824−5833.

(10) Goicoechea, J. M.; Sevov, S. C. [(Ni-Ni-Ni)@(Ge$_9$)$_2$]$^{4-}$: a linear triatomic nickel filament enclosed in a dimer of nine-atom germanium clusters. *Angew. Chem., Int. Ed.* **2005**, *44*, 4026−4028.

(11) Liu, C.; Jin, X.; Li, L.-J.; Xu, J.; McGrady, J. E.; Sun, Z.-M. Synthesis and structure of a family of rhodium polystannide clusters [Rh@Sn$_{10}$]$^{3-}$, [Rh@Sn$_{12}$]$^{3-}$, [Rh$_2$@Sn$_{17}$]$^{6-}$ and the first triply-fused stannide,[Rh$_3$@Sn$_{24}$]$^{5-}$. *Chem. Sci.* **2019**, *10*, 4394−4401.

(12) Sun, Z.-M.; Xiao, H.; Li, J.; Wang, L.-S. Pd$_2$@Sn$_{18}$$^{4-}$: Fusion of two endohedral stannaspherenes. *J. Am. Chem. Soc.* **2007**, *129*, 9560−9561.

(13) Esenturk, E. N.; Fettinger, J. C.; Eichhorn, B. W. Synthesis, structure, and dynamic properties of [Ni$_2$Sn$_{17}$]$^{4-}$. *J. Am. Chem. Soc.* **2006**, *128*, 12−13.

(14) Kesanli, B.; Halsig, J. E.; Zavalij, P.; Fettinger, J. C.; Lam, Y.-F.; Eichhorn, B. W. Cluster Growth and Fragmentation in the Highly Fluxional Platinum Derivatives of Sn$_9$$^{4-}$: Synthesis, Characterization, and Solution Dynamics of Pt$_2$@Sn$_{17}$$^{4-}$ and Pt@Sn$_9$H^{3-}. *J. Am. Chem. Soc.* **2007**, *129*, 4567−4574.

(15) Wang, J. Q.; Stegmaier, S.; Fässler, T. F. [Co@Ge$_{10}$]$^{3-}$: An intermetalloid cluster with archimedean pentagonal prismatic structure. *Angew. Chem., Int. Ed.* **2009**, *48*, 1998−2002.

(16) Zhou, B.; Denning, M. S.; Kays, D. L.; Goicoechea, J. M. Synthesis and isolation of [Fe@Ge$_{10}$]$^{3-}$: A pentagonal prismatic Zintl ion cage encapsulating an interstitial iron atom. *J. Am. Chem. Soc.* **2009**, *131*, 2802−2803.

(17) Espinoza-Quintero, G.; Duckworth, J. C.; Myers, W. K.; McGrady, J. E.; Goicoechea, J. M. Synthesis and characterization of [Ru@Ge$_{12}$]$^{3-}$: An endohedral 3-connected cluster. *J. Am. Chem. Soc.* **2014**, *136*, 1210−1213.

(18) Ugrinov, A.; Sevov, S. C. Derivatization of Deltahedral Zintl Ions by Nucleophilic Addition:[Ph-Ge$_9$-SbPh$_2$]$^{2-}$ and [Ph$_2$Sb-Ge$_9$-Ge$_9$-SbPh$_2$]$^{4-}$. *J. Am. Chem. Soc.* **2003**, *125*, 14059−14064.

(19) Hull, M. W.; Sevov, S. C. Functionalization of nine-atom deltahedral Zintl ions with organic substituents: detailed studies of the reactions. *J. Am. Chem. Soc.* **2009**, *131*, 9026−9037.

(20) Li, F.; Sevov, S. C. Rational Synthesis of [Ge$_9${Si(SiMe$_3$)$_3$}$_3$]$^-$ from Its Parent Zintl Ion Ge$_9$$^{4-}$. *Inorg. Chem.* **2012**, *51*, 2706−2708.

(21) Wallach, C.; Geitner, F. S.; Karttunen, A. J.; Fässler, T. F. Boranyl-Functionalized [Ge$_9$] Clusters: Providing the Idea of Intramolecular Ge/B Frustrated Lewis Pairs. *Angew. Chem., Int. Ed.* **2021**, *60*, 2648−2653.

(22) Kesanli, B.; Fettinger, J.; Gardner, D. R.; Eichhorn, B. The [Sn$_9$Pt$_2$(PPh$_3$)]$^{2-}$ and [Sn$_9$Ni$_2$(CO)]$^{3-}$ complexes: two markedly different Sn$_9$M$_2$L transition metal zintl ion clusters and their dynamic behavior. *J. Am. Chem. Soc.* **2002**, *124*, 4779−4786.

(23) Goicoechea, J. M.; Sevov, S. C. Deltahedral germanium clusters: Insertion of transition-metal atoms and addition of organometallic fragments. *J. Am. Chem. Soc.* **2006**, *128*, 4155−4161.

(24) Xu, L.; Sevov, S. C. Oxidative coupling of deltahedral [Ge$_9$]$^{4-}$ Zintl ions. *J. Am. Chem. Soc.* **1999**, *121*, 9245−9246.

(25) Downie, C.; Tang, Z.; Guloy, A. M. An Unprecedented (1@∞)[Ge$_9$]$^{2-}$ Polymer: A Link between Molecular Zintl Clusters and Solid-State Phases. *Angew. Chem., Int. Ed.* **2000**, *39*, 337−340.

(26) Nienhaus, A.; Hauptmann, R.; Fässler, T. F. (1@∞)-[HgGe$_9$]$^{2-}$——A Polymer with Zintl Ions as Building Blocks Covalently Linked by Heteroatoms. *Angew. Chem., Int. Ed.* **2002**, *41*, 3213−3215.

(27) Mayer, K.; Jantke, L. A.; Schulz, S.; Fässler, T. F. Retention of the Zn-Zn bond in [Ge$_9$Zn-ZnGe$_9$]$^{6-}$ and Formation of [(Ge$_9$Zn)-(Ge$_9$)-(ZnGe$_9$)]$^{8-}$ and Polymeric [-(Ge$_9$Zn)$^{2-}$−]. *Angew. Chem., Int. Ed.* **2017**, *56*, 2350−2355.

(28) Wang, J. Q.; Wahl, B.; Fässler, T. F. [Ag(Sn$_9$-Sn$_9$)]$^{5-}$: A Homoleptic Silver Complex of A Dimeric Sn$_9$ Zintl Anion. *Angew. Chem., Int. Ed.* **2010**, *49*, 6592−6595.

(29) Sevov, S. C.; Goicoechea, J. M. Chemistry of deltahedral Zintl ions. *Organometallics* **2006**, *25*, 5678−5692.

(30) Scharfe, S.; Kraus, F.; Stegmaier, S.; Schier, A.; Fässler, T. F. Zintl ions, cage compounds, and intermetalloid clusters of group 14 and group 15 elements. *Angew. Chem., Int. Ed.* **2011**, *50*, 3630−3670.

(31) Wilson, R. J.; Weinert, B.; Dehnen, S. Recent developments in Zintl cluster chemistry. *Dalton Trans.* **2018**, *47*, 14861−14869.

(32) Wilson, R. J.; Lichtenberger, N.; Weinert, B.; Dehnen, S. Intermetalloid and Heterometallic Clusters Combining p-Block (Semi)Metals with d-or f-Block Metals. *Chem. Rev.* **2019**, *119*, 8506−8554.

(33) Zhou, B.; Denning, M. S.; Chapman, T. A.; McGrady, J. E.; Goicoechea, J. M. [Pb$_9$CdCdPb$_9$]$^{6-}$: A Zintl cluster anion with an unsupported cadmium-cadmium bond. *Chem. Commun.* **2009**, 7221−7223.

(34) Goicoechea, J. M.; McGrady, J. E. On the structural landscape in endohedral silicon and germanium clusters, M@Si$_{12}$ and M@Ge$_{12}$. *Dalton Trans.* **2015**, *44*, 6755−6766.

(35) Witte, J.; Schnering, H. v.; Klemm, W. Das Verhalten der Alkalimetalle zu Halbmetallen. XI. Die Kristallstruktur von NaSi und NaGe. *Z. Anorg. Allg. Chem.* **1964**, *327*, 260−273.

(36) Wiesler, K.; Brandl, K.; Fleischmann, A.; Korber, N. Tetrahedral [Tt$_4$]$^{4-}$ Zintl Anions Through Solution Chemistry: Syntheses and Crystal Structures of the Ammoniates Rb$_4$Sn$_4$· 2NH$_3$, Cs$_4$Sn$_4$· 2NH$_3$, and Rb$_4$Pb$_4$· 2NH$_3$. *Z. Anorg. Allg. Chem.* **2009**, *635*, 508−512.

(37) Fendt, F.; Koch, C.; Gärtner, S.; Korber, N. Reaction of Sn$_4$ 4- in liquid ammonia: the formation of Rb$_6$[(η^2-Sn$_4$)Zn(η^3-Sn$_4$)]· 5NH$_3$. *Dalton Trans.* **2013**, *42*, 15548−15550.

(38) Benda, C. B.; Waibel, M.; Köchner, T.; Fässler, T. F. Reactivity of liquid ammonia solutions of the zintl phase K$_{12}$Sn$_{17}$ towards mesitylcopper (I) and phosphinegold (I) chloride. *Chem. - Eur. J.* **2014**, *20*, 16738−16746.

(39) Edwards, P. A.; Corbett, J. D. Stable homopolyatomic anions. Synthesis and crystal structures of salts containing the pentaplumbide (2-) and pentastannide (2-) anions. *Inorg. Chem.* **1977**, *16*, 903−907.

(40) Liu, C.; Li, L.-J.; Pan, Q.-J.; Sun, Z.-M. [Ge$_5$Ni$_2$(CO)$_3$]$^{2-}$: the first functionalized cluster of *closo*-[Ge$_5$]$^{2-}$. *Chem. Commun.* **2017**, *53*, 6315−6318.

(41) Tkachenko, N. V.; Boldyrev, A. I. Multiple local σ-aromaticity of nonagermanide clusters. *Chem. Sci.* **2019**, *10*, 5761−5765.

(42) Li, Y.; Mondal, K. C.; Roesky, H. W.; Zhu, H.; Stollberg, P.; Herbst-Irmer, R.; Stalke, D.; Andrada, D. M. Acyclic germylones: congeners of allenes with a central germanium atom. *J. Am. Chem. Soc.* **2013**, *135*, 12422−12428.

(43) King, R. B.; Silaghi-Dumitrescu, I.; Uţă, M. M. Density functional theory study of twelve-atom germanium clusters: conflict between the Wade-Mingos rules and optimum vertex degrees. *Dalton Trans.* **2007**, 364−372.

(44) Liu, C.; Li, L. J.; Popov, I. A.; Wilson, R. J.; Xu, C. Q.; Li, J.; Boldyrev, A. I.; Sun, Z. M. Symmetry reduction upon size mismatch: the non-icosahedral intermetalloid cluster [Co@Ge$_{12}$]$^{3-}$. *Chin. J. Chem.* **2018**, *36*, 1165−1168.

(45) Liu, C.; Popov, I. A.; Li, L. J.; Li, N.; Boldyrev, A. I.; Sun, Z. M. [Co$_2$@Ge$_{16}$]$^{4-}$: localized versus delocalized bonding in two isomeric intermetalloid clusters. *Chem. - Eur. J.* **2018**, *24*, 699−705.

(46) Gillett-Kunnath, M. M.; Paik, J. I.; Jensen, S. M.; Taylor, J. D.; Sevov, S. C. Metal-Centered Deltahedral Zintl Ions: Synthesis of [Ni@Sn$_9$]$^{4-}$ by Direct Extraction from Intermetallic Precursors and of the Vertex-Fused Dimer [{Ni@Sn$_8$(µ-Ge)$_{1/2}$}$_2$]$^{4-}$. *Inorg. Chem.* **2011**, *50*, 11695−11701.

(47) Liu, C.; Li, L.-J.; Jin, X.; McGrady, J. E.; Sun, Z.-M. Reactivity Studies of [Co@Sn$_9$]$^{4-}$ with Transition Metal Reagents: Bottom-Up Synthesis of Ternary Functionalized Zintl Clusters. *Inorg. Chem.* **2018**, *57*, 3025−3034.

(48) Stegmaier, S.; Fässler, T. F. A Bronze Matryoshka: The Discrete Intermetalloid Cluster [Sn@ Cu$_{12}$@Sn$_{20}$]$^{12-}$ in the Ternary Phases A$_{12}$Cu$_{12}$Sn$_{21}$ (A= Na, K). *J. Am. Chem. Soc.* **2011**, *133*, 19758−19768.

(49) Perla, L. G.; Sevov, S. C. Cluster Fusion: Face-Fused Nine-Atom Deltahedral Clusters in [Sn$_{14}$Ni(CO)]$^{4-}$. *Angew. Chem., Int. Ed.* **2016**, *55*, 6721−6724.

(50) Li, L.-J.; Pan, F.-X.; Li, F.-Y.; Chen, Z.-F.; Sun, Z.-M. Synthesis, characterization and electronic properties of an endohedral plumbaspherene $[Au@Pb_{12}]^{3-}$. *Inorg. Chem. Front.* **2017**, *4*, 1393−1396.

(51) Zhou, B.; Krämer, T.; Thompson, A. L.; McGrady, J. E.; Goicoechea, J. M. A Highly Distorted Open-Shell Endohedral Zintl Cluster: $[Mn@Pb_{12}]^{3-}$. *Inorg. Chem.* **2011**, *50*, 8028−8037.

(52) Li, A.-M.; Wang, Y.; Zavalij, P. Y.; Chen, F.; Muñoz-Castro, A.; Eichhorn, B. W. $[Cp*RuPb_{11}]^{3-}$ and $[Cu@Cp*RuPb_{11}]^{2-}$: centered and non-centered transition-metal substituted zintl icosahedra. *Chem. Commun.* **2020**, *56*, 10859−10862.

(53) Downing, D. O.; Liu, Z.; Eichhorn, B. W. Synthesis of $PtSn_4$ and Ir_3Sn_7 intermetallic nanoparticles from bimetallic Zintl cluster precursors. *Polyhedron* **2016**, *103*, 66−70.

(54) Wang, Y.; Zhang, C.; Wang, X.; Guo, J.; Sun, Z.-M.; Zhang, H. Site-Selective CO_2 Reduction over Highly Dispersed Ru-SnO_x Sites Derived from a $[Ru@Sn_9]^{6-}$ Zintl Cluster. *ACS Catal.* **2020**, *10*, 7808−7819.

(55) Townrow, O. P.; Chung, C.; Macgregor, S. A.; Weller, A. S.; Goicoechea, J. M. A Neutral Heteroatomic Zintl Cluster for the Catalytic Hydrogenation of Cyclic Alkenes. *J. Am. Chem. Soc.* **2020**, *142*, 18330−18335.

(56) Lichtenberger, N.; Spang, N.; Eichhöfer, A.; Dehnen, S. Between Localization and Delocalization: $Ru(cod)^{2+}$ Units in the Zintl Clusters $[Bi_9\{Ru(cod)\}_2]^{3-}$ and $[Tl_2Bi_6\{Ru(cod)\}]^{2-}$. *Angew. Chem., Int. Ed.* **2017**, *56*, 13253−13258.